Hindawi Publishing Corporation
Journal of Nanomaterials
Volume 2012, Article ID 890397, 6 pages
doi:10.1155/2012/890397

Research Article

Relationship between Crystal Shape, Photoluminescence, and Local Structure in $SrTiO_3$ Synthesized by Microwave-Assisted Hydrothermal Method

Luís F. da Silva,[1] Waldir Avansi,[2] Mário L. Moreira,[2] Alexandre Mesquita,[3] Lauro J. Q. Maia,[4] Juan Andrés,[5] Elson Longo,[2] and Valmor R. Mastelaro[1]

[1] *Instituto de Física de São Carlos, Universidade de São Paulo, 13560-970 São Carlos, SP, Brazil*
[2] *Instituto de Química, Universidade Estadual Paulista, 14800-900 Araraquara, SP, Brazil*
[3] *Departamento de Física, Universidade Federal de São Carlos, 13565-905 São Carlos, SP, Brazil*
[4] *Instituto de Física, Universidade Federal Goiás, 74001-970 Goiânia, GO, Brazil*
[5] *Departamento de Química Física y Analítica, Universitat Jaume I 12071 Castelló, Spain*

Correspondence should be addressed to Luís F. da Silva, lfsilva@ursa.ifsc.usp.br

Received 30 November 2011; Revised 1 February 2012; Accepted 15 March 2012

Academic Editor: J. C. Sczancoski

This paper describes the effect of using different titanium precursors on the synthesis and physical properties of $SrTiO_3$ powders obtained by microwave-assisted hydrothermal method. X-ray diffraction measurements, X-ray absorption near-edge structure (XANES) spectroscopy, field emission scanning electron microscopy (FE-SEM), and high-resolution transmission electron microscopy (HRTEM) were carried out to investigate the structural and optical properties of the $SrTiO_3$ spherical and cubelike-shaped particles. The appropriate choice of the titanium precursor allowed the control of morphological and photoluminescence (PL) properties of $SrTiO_3$ compound. The PL emission was more intense in $SrTiO_3$ samples composed of spherelike particles. This behavior was attributed to the existence of a lower amount of defects due to the uniformity of the spherical particles.

1. Introduction

Perovskite-type oxides are some of the most fascinating materials in condensed-matter research. Strontium titanate, $SrTiO_3$ (STO), is a representative member of this family; it displays a cubic structure and is an important *n*-type semiconductor with a band gap of approximately 3.2 eV [1].

STO has been widely studied and applied in catalyses [2], resistive oxygen gas sensors [3], solar cells [4], and random access memory [5]. Several papers have reported that its potential for technological applications is strongly related to the crystalline structure, particle size, and morphology [6–8]. Different studies have shown that the route, the precursors, and/or the parameters of synthesis appear as a key factor to control the ability to engineer crystal morphologies with desirable properties [9–12]. For example, it is well known that morphology and grain size are directly related to dielectric properties, ferroelectric polarization, and related materials [13]. Additionally, the photoluminescence (PL) properties of different perovskite oxide compounds are dependent on morphological features [7, 14–18].

The interest in compounds with perovskite-type structure that show PL properties has increased. The PL properties of disordered $ATiO_3$ compounds, synthesized by polymeric precursor method, have been extensively studied in our research group [19–25]. The origin of PL properties in these materials has been investigated by several experimental techniques and related to local order-disorder effects around Ti atoms, that is, the local disorder around the network former atom [19–23, 25].

X-ray absorption near-edge structure (XANES) spectroscopy has been employed to investigate the local structure around the titanium atoms [19–23, 25–28]. The main advantage of XANES technique is the possibility to characterize compounds without a long-order periodic structure,

specially amorphous solids. Previous studies on the Ti K-edge XANES spectra of STO amorphous samples have showed the existence of two types of Ti symmetries, fivefold (TiO_5) and sixfold (TiO_6) coordination [22]. Moreover, in the case of STO prepared by polymeric precursor method, it was observed that the reduction in the amount of TiO_5 units led to a reduction in the PL intensity [22].

Recently, PL properties have been observed in crystalline $ATiO_3$ prepared by the microwave-assisted hydrothermal (MAH) method [26, 27]. This method provides kinetic enhancement, low reaction temperature, and time reduction and generates compounds with controlled morphology and size [11, 28]. In this case, the observation of the PL property has been attributed to a tilt in the TiO_6 octahedron caused by the presence of OH^- groups and vacancies in A-site [26, 27].

The influence of synthesis parameters on the physical properties of STO samples prepared by the hydrothermal method has been widely investigated [2, 12, 29–34]. However, to the best of our knowledge, this is the first study that analyses the effect of titanium precursor on crystal-shape, photoluminescent, and structural properties of STO powders synthesized by MAH method.

Motivated by this consideration, this paper reports on the effect of using two different titanium precursors, titanium chloride and titanium oxysulfate, on the short-order local structure and optical and morphological properties of $SrTiO_3$ (STO) powders prepared by the MAH method. The STO samples were characterized by X-ray diffraction measurements, field emission scanning electron microscopy (FE-SEM), high-resolution transmission electron microscopy (HR-TEM), Ti K-edge XANES spectroscopy, and photoluminescence spectroscopy.

2. Experimental

In order to study the effect of titanium precursor, two different solutions of $SrTiO_3$ samples, denoted as SAM1 and SAM2, were prepared.

Sample 1 (SAM1) was prepared by slowly adding 0.01 mol of $TiCl_4$ (99.95%, Sigma-Aldrich) to 50 mL of cold deionized water under stirring to obtain a homogeneous solution. 0.01 mol of $SrCl_2 \cdot 2H_2O$ (99.9%, Sigma-Aldrich) was dissolved into the solution under constant stirring and purged with nitrogen gas ($12\,cm^3 \cdot min^{-1}$) at 60°C. Then, 50 mL of 6 M KOH (P.A, Sigma-Aldrich) solution was added to the precursor solution under constant stirring and nitrogen flux.

For Sample 2 (SAM2) the solution was prepared adding 0.01 mol of $TiOSO_4 \cdot xH_2SO_4 \cdot xH_2O$ (99.9%, Sigma-Aldrich) to 50 mL of warm deionized water at 60°C under continuous stirring and nitrogen flux ($12\,cm^3 \cdot min^{-1}$). In the sequence, 0.01 mol of $SrCl_2$ was dissolved into the solution and a 50 mL of 6 M KOH solution was added to the solution under stirring and nitrogen flux.

After the addition of KOH solution, each precursor solution was transferred separately in a 110 mL Teflon autoclave, sealed, and inserted in the microwave hydrothermal equipment, using a frequency of 2.45 GHz with maximum power of 800 W. The precursor solutions were heat-treated at 140°C for 10 minutes with a heating rate of $140°C \cdot min^{-1}$ and under constant pressure of 3 bar. After the synthesis, the autoclave was naturally cooled to room temperature. Then, each precipitated white powder was washed with warm deionized water for several times until attaining a neutral pH. The powder samples were dried at 80°C for 12 hours in a hot plate.

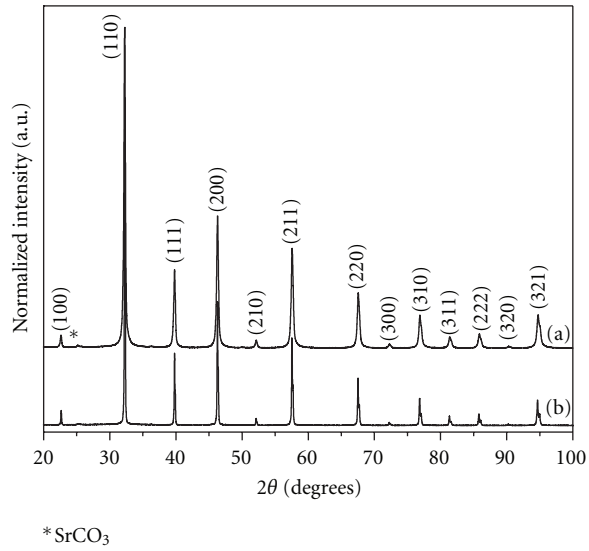

Figure 1: XRD patterns of $SrTiO_3$ powders obtained using different titanium precursors: (a) SAM1, and (b) SAM2 samples.

X-ray diffraction (XRD) measurements were taken in a Rigaku Rotaflex RU200B diffractometer, using Cu$K\alpha$ radiation. The data were collected in a 2θ range from 20 to 100° using a fixed-time mode with a 0.02° step and 5 s/point. The morphological characterization was performed by field emission scanning electron microscopy (FE-SEM, Zeiss SUPRA35) and in a transmission electron microscope (TEM, JEOL JEM 2010 URP) operating, respectively, at 5 and 200 kV. Photoluminescence (PL) spectra were collected by emission spectra obtained in a Fluorolog FL-322 Horiba/Jobin-Yvon spectrofluorimeter, with a 450 W xenon lamp for steady-state luminescence spectra and a Hamamatsu photomultiplier. The emission was corrected for the spectral response of the monochromators and by the detector using a typical correction spectrum provided by the manufacturer. STO samples were excited by 410 nm wavelength.

The titanium K-edge X-ray absorption spectra were collected at the LNLS (Brazilian Synchrotron Light Laboratory) facility using the D04B-XAS1 beamline. The LNLS storage ring was operated at 1.36 GeV and 100–160 mA. XAS spectra of grounded samples were collected at the Ti K-edge (4966 eV) in transmission mode at room temperature using Si(111) channel-cut monochromator. XANES spectra at the Ti K-edge were recorded for each sample between 4910 and 5200 eV using energy steps of 0.3 eV. Moreover, for comparison among the samples, all spectra were background

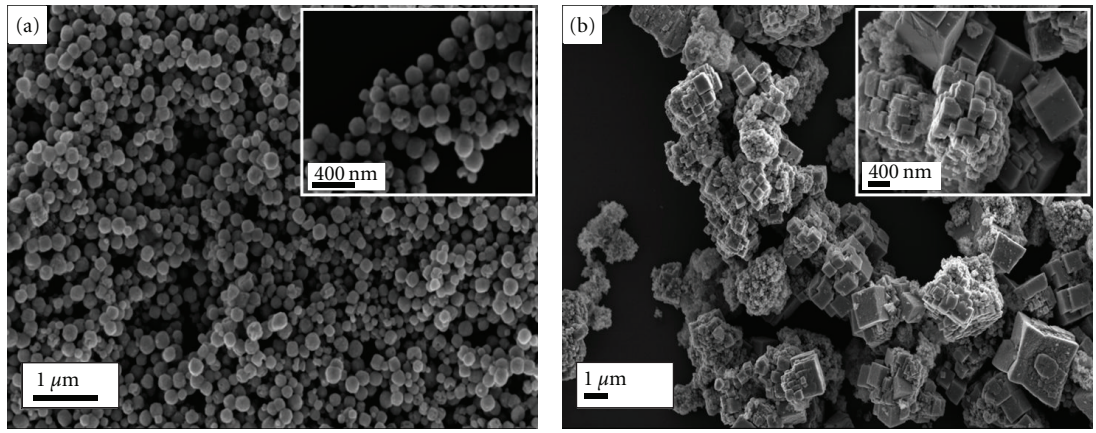

(a) (b)

Figure 2: FE-SEM images of $SrTiO_3$ powders obtained with different precursors: (a) SAM1 and (b) SAM2 samples.

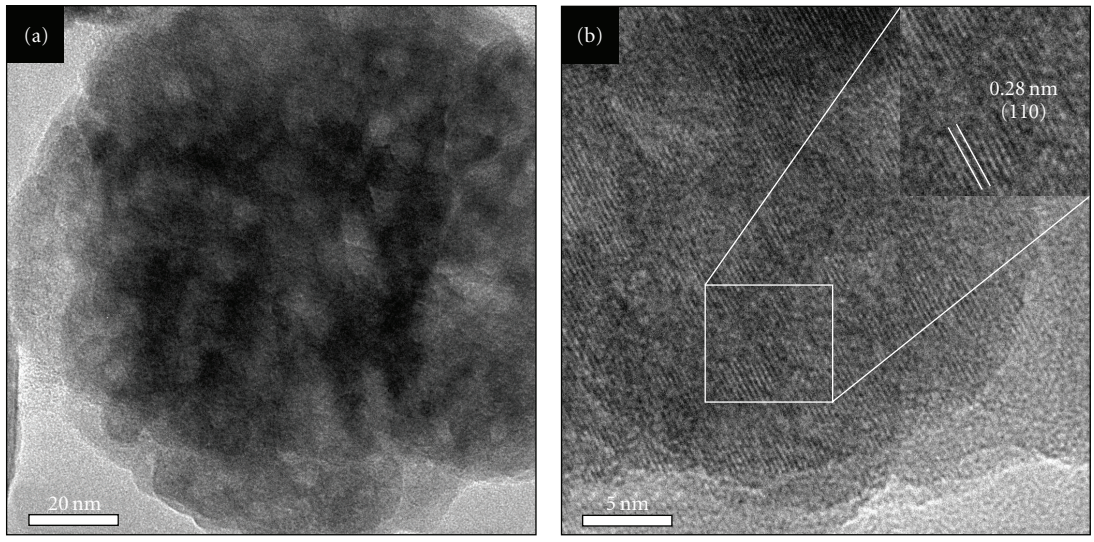

(a) (b)

Figure 3: (a) TEM and (b) HR-TEM images of the SAM1 sample.

removed and normalized using the first EXAFS (Extended X-ray Absorption Fine Structure) oscillation, as unity. XANES spectra were processed by the Multiplatform Applications for XAFS code (MAX) [35].

3. Results and Discussions

XRD patterns of STO samples prepared using different titanium precursors are presented in Figure 1. From the analysis of this figure, it is clear that all diffraction peaks are related to a cubic perovskite structure with lattice constant $a = 3.90$ Å and $Pm3m$ (221) space group (JCPDS card no: 35-0734). For SAM1 sample, a lower intensity peak related to $SrCO_3$ phase (JCPDS card no: 05-0418) was observed at 25.3°.

In order to check the morphology of STO samples synthesized with different titanium precursors, FE-SEM images were obtained. As shown in Figure 2(a), the morphology of SAM1 sample consists of STO spherical particles of ca. 150 nm, whereas the morphology of SAM2 sample consists of agglomerated particles in superstructures (~1.5 μm), exhibiting a cubelike shape. Figure 3 shows the TEM images of SAM1 sample. Although the apparent morphology of this sample has a nanospherical-like shape at around 150 nm, the TEM and HR-TEM images presented in Figures 3(a) and 3(b) reveal that these nanoparticles consist of aggregates of small nanocrystals of ca. 25 nm. From the analysis of an expanded HR-TEM image in Figure 3(b), the nanocrystal interplanar distance was determined as 0.28 nm and related to the (110) crystallographic planes of STO perovskite cubic structure, which agrees with XRD results. It is also possible to observe that the nanospherical particles present a lower contrast between the crystallites, showing the existence of nanopores separating the primary particles, already observed

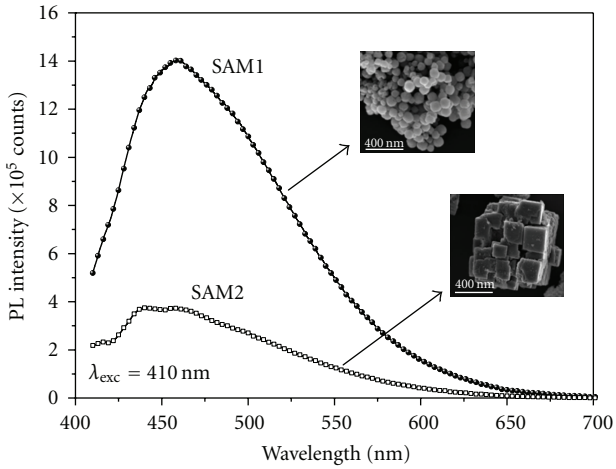

Figure 4: Room temperature photoluminescence spectra of $SrTiO_3$ samples with different shapes.

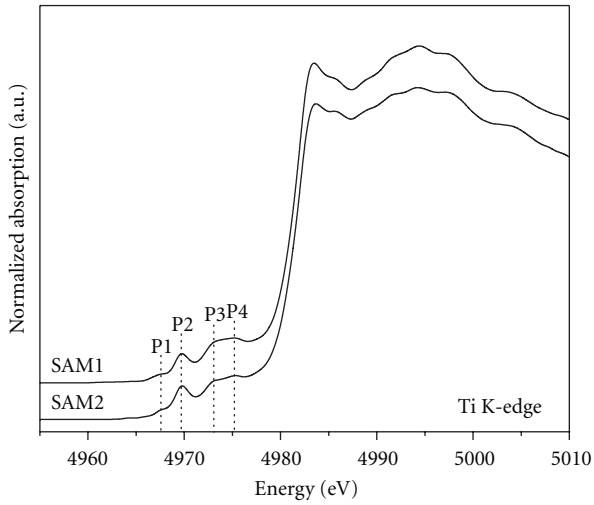

Figure 5: Ti K-edge XANES spectra of $SrTiO_3$ samples.

during the process of STO nanostructures growth [36, 37]. Calderone and co-workers studied the synthesis of STO nanostructures by coprecipitation method and proposed that the aggregates were composed of small nanocrystals originated from an oriented attachment assisted by the self-assembly process of small primary nanocrystals [32]. As seen in the TEM images of SAM1 sample, the aggregation of these small particles is irreversible and occurs in a highly oriented manner, leading to the elimination of the interface of adjacent crystals. This growth mechanism has been also observed in several compounds synthesized by hydrothermal method [10, 38–40].

Figure 4 shows the photoluminescence (PL) emission spectra at room temperature of SAM1 (spherelike) and SAM2 (cubelike) samples. The PL spectra exhibit a broad blue emission centered at 460 nm for SAM1 sample and between 440 and 460 nm for SAM2 sample. Comparing both samples, it is clear that the SAM1 sample shows a higher emission intensity compared to SAM2. This behavior has been observed in samples with particles that exhibit a spherical geometry and higher emission intensity than particles with other morphologies [7, 15, 17]. According to these studies, the intrinsic geometry of the spherical particles minimizes the scattering of light from the particle surfaces in comparison to a cube-shaped particle [7, 15, 17]. Besides, the enhancement of the PL emission can also be attributed to a reduction in the surface defects and the higher uniformity in shape of the superstructures [7, 14, 17].

Several papers have reported the relationship between the local order structure of titanium atoms and the photoluminescent properties of titanate compounds synthesized by polymeric precursor method [19, 20, 22, 23, 25]. According to Longo and co-workers, the reduction in the PL intensity in function of the annealing temperature of STO samples is due to a reduction in the local disorder around titanium atoms [22]. In order to check the dependence of the local order structure of the studied samples and the behavior of PL as a function of titanium precursor, Ti K-edge XANES spectra of STO samples were measured and are shown in Figure 5. These spectra present four pre-edge transitions labeled P1, P2, P3, and P4. Transition P1 is caused by a quadrupole excitation of 1*s* electron to t_{2g} orbitals of the TiO_6 octahedron [41], while transition P2 occurs due to the 1*s* electron transition to the unoccupied 3*d* level; this forbidden electronic transition can be allowed if there occurs a mixture of oxygen 2*p* states and empty titanium 3*d* states [27, 42]. The intensity of peak P2 has shown to be sensitive to the local structure around titanium atoms [19, 43]. Transitions P3 and P4 are assigned to the dipole excitation of the 1*s* electron into the t_{2g} and e_g orbitals of the neighboring TiO_6 octahedra [41, 44].

As observed in Figure 5, Ti K-edge XANES spectra of SAM1 and SAM2 samples are very similar, especially in the pre-edge region (4960 to 4980 eV), with a pre-edge typical of sixfold coordination (TiO_6) compounds [22, 45]. Moreover, after the edge, the oscillations observed in both samples are also quite similar, indicating the same neighborhood around the titanium atoms. Based on the analysis of the XANES spectra, it can be stated that the titanium atoms local symmetry, that is, the TiO_6 octahedra, and the medium-range order around titanium atoms are not affected by the use of different titanium precursors employed in the synthesis of STO powders. This result has confirmed that the variation observed in the PL emission is more related to the particle morphology of SAM1 and SAM2 samples.

4. Conclusion

This study has evidenced that an appropriate selection of titanium precursor allows a control of morphology and PL property of STO powders obtained by using the microwave-hydrothermal method. The use of titanium chloride as the precursor leads to the formation of STO samples of spherical morphology, whereas cubelike particles are formed by the spontaneous assembly of small primary nanocrystals when titanium oxysulfate is used as a precursor. The analysis of XANES spectra allowed observing that change in the crystal

morphology does not affect the local order symmetry of TiO_6 octahedra as well as the medium range order around titanium atoms. The PL emission was more intense in spherelike particles in comparison to cubelike particles. This behavior was attributed to the existence of a lower amount of defects due to the uniformity of the spherical particles.

Acknowledgments

The authors are greatful to Mr. Rorivaldo Camargo for operating the FE-SEM equipment. They also acknowledge the financial support of the Brazilian research funding institution CNPq (Proc.MCT/CNPq no. 70/2008) and FAPESP. The XAS measurements and HR-TEM microscopy facilities were provided by the Brazilian Laboratory of Synchrotron Radiation (LNLS). J. Andrés acknowledges Generalitat Valenciana (Prometeo/2009/053 project), Ministerio de Ciencia e Innovación (CTO2009-14541-C02 project) Programa de Cooperación Científica con Iberoamerica (Brasil), Ministerio de Educación (PHB2009-0065-PC project).

References

[1] M. Cardona, "Optical properties and band structure of $SrTiO_3$ and $BaTiO_3$," *Physical Review*, vol. 140, no. 2A, pp. A651–A655, 1965.

[2] Z. K. Zheng, B. B. Huang, X. Y. Qin, X. Y. Zhang, and Y. Dai, "Facile synthesis of $SrTiO_3$ hollow microspheres built as assembly of nanocubes and their associated photocatalytic activity," *Journal of Colloid and Interface Science*, vol. 358, no. 1, pp. 68–72, 2011.

[3] F. Voigts, T. Damjanovic, G. Borchardt, C. Argirusis, and W. Maus-Friedrichs, "Synthesis and characterization of strontium titanate nanoparticles as potential high temperature oxygen sensor material," *Journal of Nanomaterials*, vol. 2006, Article ID 63154, pp. 1–6, 2006.

[4] S. Burnside, J. E. Moser, K. Brooks, M. Gratzel, and D. Cahen, "Nanocrystalline mesoporous strontium titanate as photoelectrode material for photosensitized solar devices: increasing photovoltage through flatband potential engineering," *Journal of Physical Chemistry B*, vol. 103, no. 43, pp. 9328–9332, 1999.

[5] R. Waser and M. Aono, "Nanoionics-based resistive switching memories," *Nature Materials*, vol. 6, no. 11, pp. 833–840, 2007.

[6] L. F. da Silva, L. J. Q. Maia, M. I. B. Bernardi, J. A. Andres, and V. R. Mastelaro, "An improved method for preparation of $SrTiO_3$ nanoparticles," *Materials Chemistry and Physics*, vol. 125, no. 1-2, pp. 168–173, 2011.

[7] H. J. Zhou, Y. B. Mao, and S. S. Wong, "Shape control and spectroscopy of crystalline $BaZrO_3$ perovskite particles," *Journal of Materials Chemistry*, vol. 17, pp. 1707–1713, 2007.

[8] Y. Hu, O. K. Tan, and W. G. Zhu, "Nanosized metal-oxide semiconducting $SrTi_{1\pm x}O_{3-\delta}$ oxygen gas sensors for low-temperature application," *IEEE Sensors Journal*, vol. 6, no. 6, pp. 1389–1394, 2006.

[9] M. Alfredsson, F. Cora, D. P. Dobson et al., "Dopant control over the crystal morphology of ceramic materials," *Surface Science*, vol. 601, no. 21, pp. 4793–4800, 2007.

[10] C. J. Dalmaschio, C. Ribeiro, and E. R. Leite, "Impact of the colloidal state on the oriented attachment growth mechanism," *Nanoscale*, vol. 2, no. 11, pp. 2336–2345, 2010.

[11] I. Bilecka and M. Niederberger, "Microwave chemistry for inorganic nanomaterials synthesis," *Nanoscale*, vol. 2, no. 8, pp. 1358–1374, 2010.

[12] W. Dong, B. Li, Y. Li et al., "General approach to well-defined perovskite $MTiO_3$ (M = Ba, Sr, Ca, and Mg) nanostructures," *Journal of Physical Chemistry C*, vol. 115, no. 10, pp. 3918–3925, 2011.

[13] S. Berger and Y. Drezner, "Nano-domains in thin $BaTiO_3$ films," *Ferroelectrics* , vol. 327, no. 1, pp. 85–89, 2005.

[14] C. Xu, D. B. Zou, H. Guo, F. Jie, and T. K. Ying, "Luminescence properties of hierarchical $CaMoO_4$ microspheres derived by ionic liquid-assisted process," *Journal of Luminescence*, vol. 129, no. 5, pp. 474–477, 2009.

[15] L. Xu, C. L. Lu, Z. H. Zhang, X. Y. Yang, and W. H. Hou, "Various self-assembled three-dimensional hierarchical architectures of $La_2(MoO_4)_3$: controlled synthesis, growth mechanisms, luminescence properties and adsorption activities," *Nanoscale*, vol. 2, no. 6, pp. 995–1005, 2010.

[16] W. S. Wang, Y. X. Hu, J. Goebl, Z. D. Lu, L. Zhen, and Y. D. Yin, "Shape-and size-controlled synthesis of calcium molybdate doughnut-shaped microstructures," *Journal of Physical Chemistry C*, vol. 113, no. 37, pp. 16414–16423, 2009.

[17] Z. G. Lu, Y. G. Tang, L. M. Chen, and Y. D. Li, "Shape-controlled synthesis and characterization of $BaZrO_3$ microcrystals," *Journal of Crystal Growth*, vol. 266, no. 4, pp. 539–544, 2004.

[18] A. Kar, S. Kundu, and A. Patra, "Surface defect-related luminescence properties of SnO_2 nanorods and nanoparticles," *Journal of Physical Chemistry C*, vol. 115, no. 1, pp. 118–124, 2011.

[19] S. de Lazaro, J. Milanez, A. T. de Figueiredo et al., "Relation between photoluminescence emission and local order-disorder in the $CaTiO_3$ lattice modifier," *Applied Physics Letters*, vol. 90, no. 11, Article ID 111904, 3 pages, 2007.

[20] A. T. de Figueiredo, V. M. Longo, S. de Lazaro et al., "Blue-green and red photoluminescence in $CaTiO_3$: Sm," *Journal of Luminescence*, vol. 126, no. 2, pp. 403–407, 2007.

[21] E. Longo, A. T. de Figueiredo, M. S. Silva et al., "Influence of structural disorder on the photoluminescence emission of PZT powder," *Journal of Physical Chemistry A*, vol. 112, no. 38, pp. 8953–8957, 2008.

[22] V. M. Longo, A. T. de Figueiredo, S. de Lazaro et al., "Structural conditions that leads to photoluminescence emission in $SrTiO_3$: an experimental and theoretical approach," *Journal of Applied Physics*, vol. 104, no. 2, Article ID 023515, 11 pages, 2008.

[23] F. M. Pontes, E. Longo, E. R. Leite et al., "Photoluminescence at room temperature in amorphous $SrTiO_3$ thin films obtained by chemical solution deposition," *Materials Chemistry and Physics*, vol. 77, no. 2, pp. 598–602, 2003.

[24] L. Gracia, J. Andres, V. M. Longo, J. A. Varela, and E. Longo, "A theoretical study on the photoluminescence of $SrTiO_3$," *Chemical Physics Letters*, vol. 493, no. 1–3, pp. 141–146, 2010.

[25] E. A. V. Ferri, J. C. Sczancoski, L. S. Cavalcante et al., "Photoluminescence behavior in $MgTiO_3$ powders with vacancy/distorted clusters and octahedral tilting," *Materials Chemistry and Physics*, vol. 117, no. 1, pp. 192–198, 2009.

[26] M. L. Moreira, G. P. Mambrini, D. P. Volanti et al., "Hydrothermal microwave: a new route to obtain photoluminescent crystalline $BaTiO_3$ nanoparticles," *Chemistry of Materials*, vol. 20, no. 16, pp. 5381–5387, 2008.

[27] M. L. Moreira, E. C. Paris, G. S. do Nascimento et al., "Structural and optical properties of $CaTiO_3$ perovskite-based materials obtained by microwave-assisted hydrothermal synthesis:

an experimental and theoretical insight," *Acta Materialia*, vol. 57, no. 17, pp. 5174–5185, 2009.

[28] M. L. Moreira, J. Andres, J. A. Varela, and E. Longo, "Synthesis of fine micro-sized $BaZrO_3$ powders based on a decaoctahedron shape by the microwave-assisted hydrothermal method," *Crystal Growth and Design*, vol. 9, no. 2, pp. 833–839, 2009.

[29] W. Dong, X. Li, J. Yu et al., "Porous $SrTiO_3$ spheres with enhanced photocatalytic performance," *Materials Letters*, vol. 67, no. 1, pp. 131–134, 2012.

[30] Y. M. Rangel-Hernandez, J. C. Rendon-Angeles, Z. Matamoros-Veloza, M. I. Pech-Canul, S. Diaz-de la Torre, and K. Yanagisawa, "One-step synthesis of fine $SrTiO_3$ particles using $SrSO_4$ ore under alkaline hydrothermal conditions," *Chemical Engineering Journal*, vol. 155, no. 1-2, pp. 483–492, 2009.

[31] Y. Li, X. P. Gao, G. L. Pan, G. R. Li, T. Y. Yan, and H. Y. Zhu, "Titanate nanofiber reactivity: fabrication of $MTiO_3$ (M = Ca, Sr, and Ba) perovskite oxides," *Journal of Physical Chemistry C*, vol. 113, no. 11, pp. 4386–4394, 2009.

[32] V. R. Calderone, A. Testino, M. T. Buscaglia et al., "Size and shape control of $SrTiO_3$ particles grown by epitaxial self-assembly," *Chemistry of Materials*, vol. 18, no. 6, pp. 1627–1633, 2006.

[33] H. Xu, S. Wei, H. Wang, M. Zhu, R. Yu, and H. Yan, "Preparation of shape controlled $SrTiO_3$ crystallites by sol-gel-hydrothermal method," *Journal of Crystal Growth*, vol. 292, no. 1, pp. 159–164, 2006.

[34] X. Wei, G. Xu, Z. Ren et al., "Single-crystal-like mesoporous $SrTiO_3$ spheres with enhanced photocatalytic performance," *Journal of the American Ceramic Society*, vol. 93, no. 5, pp. 1297–1305, 2010.

[35] A. Michalowicz, J. Moscovici, D. Muller-Bouvet, and K. Provost, "MAX: multiplatform applications for XAFS," in *Proceedings of the 14th International Conference on X-Ray Absorption Fine Structure*, A. DiCicco and A. Filipponi, Eds., Iop Publishing, Camerino, Italy, 2009.

[36] F. A. Rabuffetti, H. S. Kim, J. A. Enterkin et al., "Synthesis-dependent first-order Raman scattering in $SrTiO_3$ nanocubes at room temperature," *Chemistry of Materials*, vol. 20, no. 17, pp. 5628–5635, 2008.

[37] W. Avansi Jr., C. Ribeiro, E. R. Leite, and V. R. Mastelaro, "Growth kinetics of vanadium pentoxide nanostructures under hydrothermal conditions," *Journal of Crystal Growth*, vol. 312, no. 23, pp. 3555–3559, 2010.

[38] M. Niederberger and H. Colfen, "Oriented attachment and mesocrystals: non-classical crystallization mechanisms based on nanoparticle assembly," *Physical Chemistry Chemical Physics*, vol. 8, no. 28, pp. 3271–3287, 2006.

[39] M. L. Moreira, J. Andres, V. R. Mastelaro, J. A. Varela, and E. Longo, "On the reversed crystal growth of $BaZrO_3$ decaoctahedron: shape evolution and mechanism," *CrystEngComm* , vol. 13, no. 19, pp. 5818–5824, 2011.

[40] C. Ribeiro, C. Vila, D. B. Stroppa et al., "Anisotropic growth of oxide nanocrystals: Insights into the rutile TiO_2 phase," *Journal of Physical Chemistry C*, vol. 111, no. 16, pp. 5871–5875, 2007.

[41] P. P. Neves, A. C. Doriguetto, V. R. Mastelaro et al., "XAS and XRD structural characterization of lanthanum-modified $PbTiO_3$ ceramic materials," *Journal of Physical Chemistry B*, vol. 108, no. 39, pp. 14840–14849, 2004.

[42] F. Farges, G. E. Brown, and J. J. Rehr, "Ti K-edge XANES studies of Ti coordination and disorder in oxide compounds: comparison between theory and experiment," *Physical Review B*, vol. 56, no. 4, pp. 1809–1819, 1997.

[43] R. V. Vedrinskii, V. L. Kraizman, A. A. Novakovich, P. V. Demekhin, and S. V. Urazhdin, "Pre-edge fine structure of the 3d atom K X-ray absorption spectra and quantitative atomic structure determinations for ferroelectric perovskite structure crystals," *Journal of Physics Condensed Matter*, vol. 10, no. 42, pp. 9561–9580, 1998.

[44] T. Yamamoto, T. Mizoguchi, and I. Tanaka, "Core-hole effect on dipolar and quadrupolar transitions of $SrTiO_3$ and $BaTiO_3$ at Ti K edge," *Physical Review B*, vol. 71, no. 24, Article ID 245113, 4 pages, 2005.

[45] T. Yamamoto, "Assignment of pre-edge peaks in K-edge X-ray absorption spectra of 3D transition metal compounds: electric dipole or quadrupole?" *X-ray Spectrom*, vol. 37, pp. 572–584, 2008.